Eur. Phys. J. C 49, 511–522 (2007)
DOI 10.1140/epjc/s10052-006-0134-1

THE EUROPEAN PHYSICAL JOURNAL C

Regular Article – Experimental Physics

# Measurement of prompt photons with associated jets in photoproduction at HERA

The ZEUS Collaboration

S. Chekanov[1], M. Derrick[1], S. Magill[1], S. Miglioranzi[1,52], B. Musgrave[1], D. Nicholass[1,53], J. Repond[1], R. Yoshida[1], M.C.K. Mattingly[2], N. Pavel[3,a], A.G. Yagües Molina[3], S. Antonelli[4], P. Antonioli[4], G. Bari[4], M. Basile[4], L. Bellagamba[4], M. Bindi[4], D. Boscherini[4], A. Bruni[4], G. Bruni[4], L. Cifarelli[4], F. Cindolo[4], A. Contin[4], M. Corradi[4,54,b] i, S. De Pasquale[4], G. Iacobucci[4], A. Margotti[4], R. Nania[4], A. Polini[4], L. Rinaldi[4], G. Sartorelli[4], A. Zichichi[4], G. Aghuzumtsyan[5], D. Bartsch[5], I. Brock[5], S. Goers[5], H. Hartmann[5], E. Hilger[5], H.-P. Jakob[5], M. Jüngst[5], O.M. Kind[5], E. Paul[5,c], J. Rautenberg[5,55], R. Renner[5], U. Samson[5,d], V. Schönberg[5], M. Wang[5], M. Wlasenko, N.H. Brook[6], G.P. Heath[6], J.D. Morris[6], T. Namsoo, M. Capua[7], S. Fazio[7], A. Mastroberardino[7], M. Schioppa[7], G. Susinno[7], E. Tassi[7], J.Y. Kim[8,e], K.J. Ma[8,f], Z.A. Ibrahim[9], B. Kamaluddin[9], W.A.T. Wan Abdullah[9], Y. Ning[10], Z. Ren[10], F. Sciulli[10], J. Chwastowski[11], A. Eskreys[11], J. Figiel[11], A. Galas[11], M. Gil[11], K. Olkiewicz[11], P. Stopa[11], L. Zawiejski[11], L. Adamczyk[12], T. Bołd[12], I. Grabowska-Bołd[12], D. Kisielewska[12], J. Łukasik[12], M. Przybycień[12], L. Suszycki[12], A. Kotański[13,g], W. Słomiński[13], V. Adler[14], U. Behrens[14], I. Bloch[14], A. Bonato[14], K. Borras[14], N. Coppola[14], J. Fourletova[14], A. Geiser[14], D. Gladkov[14], P. Göttlicher[14,56], I. Gregor[14], O. Gutsche[14], T. Haas[14], W. Hain[14], C. Horn[14], B. Kahle[14], U. Kötz[14], H. Kowalski[14], H. Lim[14,57], E. Lobodzinska[14], B. Löhr[14], R. Mankel[14], I.-A. Melzer-Pellmann[14], A. Montanari[14], C.N. Nguyen[14], D. Notz[14], A.E. Nuncio-Quiroz[14], R. Santamarta[14], U. Schneekloth[14], A. Spiridonov[14,58], H. Stadie[14], U. Stösslein[14], D. Szuba[14,59], J. Szuba[14,60], T. Theedt[14], G. Watt[14], G. Wolf[14], K. Wrona[14], C. Youngman[14], W. Zeuner[14], S. Schlenstedt[15], G. Barbagli[16], E. Gallo[16], P. G. Pelfer[16], A. Bamberger[17], D. Dobur[17], F. Karstens[17], N.N. Vlasov[17,h], P.J. Bussey[18], A.T. Doyle[18], W. Dunne[18], J. Ferrando[18], D.H. Saxon[18], I.O. Skillicorn[18], I. Gialas[19,61], T. Gosau[20], U. Holm[20], R. Klanner[20], E. Lohrmann[20], H. Salehi[20], P. Schleper[20], T. Schörner-Sadenius[20], J. Sztuk[20], K. Wichmann[20], K. Wick[20], C. Foudas[21], C. Fry[21], K.R. Long[21], A.D. Tapper[21], M. Kataoka[22,62], T. Matsumoto[22], K. Nagano[22], K. Tokushuku[22,63], S. Yamada[22], Y. Yamazaki[22], A.N. Barakbaev[23], E.G. Boos[23], A. Dossanov[23], N.S. Pokrovskiy[23], B.O. Zhautykov[23], D. Son[24], J. de Favereau[25], K. Piotrzkowski[25], F. Barreiro[26], C. Glasman[26,i], M. Jimenez[26], L. Labarga[26], J. del Peso[26], E. Ron[26], J. Terrón[26], M. Zambrana[26], F. Corriveau[27], C. Liu[27], R. Walsh[27], C. Zhou[27], T. Tsurugai[28], A. Antonov[29], B.A. Dolgoshein[29], I. Rubinsky[29], V. Sosnovtsev[29], A. Stifutkin[29], S. Suchkov[29], R.K. Dementiev[30], P.F. Ermolov[30], L.K. Gladilin[30], I.I. Katkov[30], L.A. Khein[30], I.A. Korzhavina[30], V.A. Kuzmin[30], B.B. Levchenko[30,j], O.Y. Lukina[30], A.S. Proskuryakov[30], L.M. Shcheglova[30], D.S. Zotkin[30], S.A. Zotkin[30], N.P. Zotov[30], I. Abt[31], C. Büttner[31], A. Caldwell[31], D. Kollar[31], W.B. Schmidke[31], J. Sutiak[31], G. Grigorescu[32], A. Keramidas[32], E. Koffeman[32], P. Kooijman[32], A. Pellegrino[32], H. Tiecke[32], M. Vázquez[32,64], L. Wiggers[32], N. Brümmer[33], B. Bylsma[33], L.S. Durkin[33], A. Lee[33], T.Y. Ling[33], P.D. Allfrey[34], M.A. Bell[34], A.M. Cooper-Sarkar[34], A. Cottrell[34], R.C.E. Devenish[34], B. Foster[34], C. Gwenlan[34,k], K. Korcsak-Gorzo[34], S. Patel[34], V. Roberfroid[34,l], A. Robertson[34], P.B. Straub[34], C. Uribe-Estrada[34], R. Walczak[34], P. Bellan[35], A. Bertolin[35], R. Brugnera[35], R. Carlin[35], R. Ciesielski[35], F. Dal Corso[35], S. Dusini[35], A. Garfagnini[35], S. Limentani[35], A. Longhin[35], L. Stanco[35], M. Turcato[35], B.Y. Oh[36], A. Raval[36], J.J. Whitmore[36], Y. Iga[37], G. D'Agostini[38], G. Marini[38], A. Nigro[38], J.E. Cole[39], J.C. Hart[39], H. Abramowicz[40,65], A. Gabareen[40], R. Ingbir[40], S. Kananov[40], A. Levy[40], M. Kuze[41], R. Hori[42], S. Kagawa[42,66], S. Shimizu[42], T. Tawara[42], R. Hamatsu[43], H. Kaji[43], S. Kitamura[43,67], O. Ota[43], Y.D. Ri[43], M.I. Ferrero[44], V. Monaco[44], R. Sacchi[44], A. Solano[44], M. Arneodo[45], M. Ruspa[45], S. Fourletov[46], J.F. Martin[46], S.K. Boutle[4761], J.M. Butterworth[47], R. Hall-Wilton[47,64], T.W. Jones[47], J.H. Loizides[47], M.R. Sutton[47,m], C. Targett-Adams[47], M. Wing[47], B. Brzozowska[48], J. Ciborowski[48,68], G. Grzelak[48], P. Kulinski[48], P. Łużniak[48,69], J. Malka[48,69], R.J. Nowak[48], J.M. Pawlak[48], T. Tymieniecka[48], A. Ukleja[48,n], J. Ukleja[48,o], A.F. Żarnecki[48], M. Adamus[49], P. Plucinski[49,p], Y. Eisenberg[50], I. Giller[50], D. Hochman[50], U. Karshon[50], M. Rosin[50], E. Brownson[51], T. Danielson[51], A. Everett[51], D. Kçira[51], D.D. Reeder[51], P. Ryan[51], A.A. Savin[51], W.H. Smith[51], H. Wolfe[51], S. Bhadra[52], C.D. Catterall[52], Y. Cui[52], G. Hartner[52], S. Menary[52], U. Noor[52], M. Soares[52], J. Standage[52], J. Whyte[52]

[1] Argonne National Laboratory, Argonne, IL 60439-4815, USA[q]
[2] Andrews University, Berrien Springs, MI 49104-0380, USA
[3] Institut für Physik der Humboldt-Universität zu Berlin, Berlin, Germany
[4] University and INFN Bologna, Bologna, Italy[r]

[5] Physikalisches Institut der Universität Bonn, Bonn, Germany[s]
[6] H.H. Wills Physics Laboratory, University of Bristol, Bristol, UK[t]
[7] Calabria University, Physics Department and INFN, Cosenza, Italy[u]
[8] Chonnam National University, Kwangju, South Korea[u]
[9] Jabatan Fizik, Universiti Malaya, 50603 Kuala Lumpur, Malaysia[v]
[10] Nevis Laboratories, Columbia University, Irvington on Hudson, NY 10027, USA[w]
[11] The Henryk Niewodniczanski Institute of Nuclear Physics, Polish Academy of Sciences, Cracow, Poland[x]
[12] Faculty of Physics and Applied Computer Science, AGH-University of Science and Technology, Cracow, Poland[y]
[13] Department of Physics, Jagellonian University, Cracow, Poland
[14] Deutsches Elektronen-Synchrotron DESY, Hamburg, Germany
[15] Deutsches Elektronen-Synchrotron DESY, Zeuthen, Germany
[16] University and INFN, Florence, Italy[u]
[17] Fakultät für Physik der Universität Freiburg i.Br., Freiburg i.Br., Germany[r]
[18] Department of Physics and Astronomy, University of Glasgow, Glasgow, UK[ac]
[19] Department of Engineering in Management and Finance, Univ. of Aegean, Greece
[20] Hamburg University, Institute of Exp. Physics, Hamburg, Germany[r]
[21] Imperial College London, High Energy Nuclear Physics Group, London, UK[ac]
[22] Institute of Particle and Nuclear Studies, KEK, Tsukuba, Japan[z]
[23] Institute of Physics and Technology of Ministry of Education and Science of Kazakhstan, Almaty, Kazakhstan
[24] Kyungpook National University, Center for High Energy Physics, Daegu, South Korea[w]
[25] Institut de Physique Nucléaire, Université Catholique de Louvain, Louvain-la-Neuve, Belgium[aa]
[26] Departamento de Física Teórica, Universidad Autónoma de Madrid, Madrid, Spain[ab]
[27] Department of Physics, McGill University, Montréal, Québec, Canada H3A 2T8[ac]
[28] Meiji Gakuin University, Faculty of General Education, Yokohama, Japan[v]
[29] Moscow Engineering Physics Institute, Moscow, Russia[ad]
[30] Moscow State University, Institute of Nuclear Physics, Moscow, Russia[ae]
[31] Max-Planck-Institut für Physik, München, Germany
[32] NIKHEF and University of Amsterdam, Amsterdam, Netherlands[af]
[33] Physics Department, Ohio State University, Columbus, OH 43210, USA[ad]
[34] Department of Physics, University of Oxford, Oxford, UK[ac]
[35] Dipartimento di Fisica dell' Università and INFN, Padova, Italy[u]
[36] Department of Physics, Pennsylvania State University, University Park, PA 16802, USA[ae]
[37] Polytechnic University, Sagamihara, Japan[v]
[38] Dipartimento di Fisica, Università 'La Sapienza' and INFN, Rome, Italy[u]
[39] Rutherford Appleton Laboratory, Chilton, Didcot, Oxon, UK[ac]
[40] Raymond and Beverly Sackler Faculty of Exact Sciences, School of Physics, Tel-Aviv University, Tel-Aviv, Israel[ag]
[41] Department of Physics, Tokyo Institute of Technology, Tokyo, Japan[v]
[42] Department of Physics, University of Tokyo, Tokyo, Japan[v]
[43] Tokyo Metropolitan University, Department of Physics, Tokyo, Japan[v]
[44] Università di Torino and INFN, Torino, Italy[u]
[45] Università del Piemonte Orientale, Novara, and INFN, Torino, Italy[u]
[46] Department of Physics, University of Toronto, Toronto, Ontario, Canada M5S 1A7[q]
[47] Physics and Astronomy Department, University College London, London, UK[ac]
[48] Warsaw University, Institute of Experimental Physics, Warsaw, Poland
[49] Institute for Nuclear Studies, Warsaw, Poland
[50] Department of Particle Physics, Weizmann Institute, Rehovot, Israel[ah]
[51] Department of Physics, University of Wisconsin, Madison, WI 53706, USA[ad]
[52] Department of Physics, York University, Ontario, Canada M3J 1P3[q]
[53] also affiliated with University College London, UK
[54] also at University of Hamburg, Hamburg, Germany, Alexander von Humboldt Fellow
[55] now at Univ. of Wuppertal, Germany
[56] now at DESY group FEB, Hamburg, Germany
[57] now at Argonne National Laboratory, Argonne, IL, USA
[58] also at Institut of Theoretical and Experimental Physics, Moscow, Russia
[59] also at INP, Cracow, Poland
[60] on leave of absence from FPACS, AGH-UST, Cracow, Poland
[61] also affiliated with DESY, Hamburg, Germany
[62] now at ICEPP, University of Tokyo, Japan
[63] also at University of Tokyo, Japan
[64] now at CERN, Geneva, Switzerland
[65] also at Max Planck Institute, Munich, Germany, Alexander von Humboldt Research Award
[66] now at KEK, Tsukuba, Japan

[67] Tokyo Metropolitan University, Department of Radiological Science, Tokyo, Japan
[68] also at Łódź University, Poland
[69] Łódź University, Poland

Received: 10 August 2006 / Revised version: 26 September 2006 /
Published online: 8 November 2006 – © Springer-Verlag / Società Italiana di Fisica 2006

**Abstract.** The photoproduction of prompt photons, together with an accompanying jet, has been studied in $ep$ collisions at a centre-of-mass energy of 318 GeV with the ZEUS detector at HERA using an integrated luminosity of $77\,\mathrm{pb}^{-1}$. Cross sections were measured for the transverse energy of the photon and the jet larger than 5 and 6 GeV, respectively. The differential $\gamma$+jet cross sections were reconstructed as functions of the transverse energy, pseudorapidity and $x_\gamma^{\mathrm{obs}}$, the fraction of the incoming photon momentum taken by the photon-jet system. Predictions based on leading-logarithm parton-shower Monte Carlo models and next-to-leading-order (NLO) QCD generally underestimate the cross sections for the transverse energies of prompt photons below 7 GeV, while the $k_{\mathrm{T}}$-factorisation QCD calculation agrees with the data better. When the minimum transverse energy of prompt photons is increased to 7 GeV, both NLO QCD and the $k_{\mathrm{T}}$-factorisation calculations are in good agreement with the data.

## 1 Introduction

Events containing an isolated photon (prompt photon) are a powerful tool to study hard interaction processes since such photons emerge without the hadronisation phase by which a final state quark or gluon forms a jet. In $ep$ collisions, the presence of a jet in addition to the photon allows measurements that are more sensitive to the underlying partonic processes than is possible for inclusive prompt-photon events. In particular, final states with a prompt photon with a high transverse energy ($E_{\mathrm{T}}$) together with a high-$E_{\mathrm{T}}$ jet are directly sensitive to the quark content of the proton through the scattering of the exchanged photon with a quark, $\gamma q \to \gamma q$ (Compton scattering). In this case, the incident photon is point like, and the process (Fig. 1a and b) is called direct. For exchanged four-momentum transfer close

[a] deceased
[b] e-mail: corradi@mail.desy.de
[c] retired
[d] formerly U. Meyer
[e] supported by Chonnam National University in 2005
[f] supported by a scholarship of the World Laboratory Björn Wiik Research Project
[g] supported by the research grant no. 1 P03B 04529 (2005–2008)
[h] partly supported by Moscow State University, Russia
[i] Ramón y Cajal Fellow
[j] partly supported by Russian Foundation for Basic Research grant no. 05-02-39028-NSFC-a
[k] PPARC Postdoctoral Research Fellow
[l] EU Marie Curie Fellow
[m] PPARC Advanced fellow
[n] supported by the Polish Ministry for Education and Science grant no. 1 P03B 12629
[o] supported by the KBN grant no. 2 P03B 12725
[p] supported by the Polish Ministry for Education and Science grant no. 1 P03B 14129
[q] supported by the US Department of Energy
[r] supported by the Italian National Institute for Nuclear Physics (INFN)
[s] supported by the German Federal Ministry for Education and Research (BMBF), under contract numbers HZ1GUA 2, HZ1GUB 0, HZ1PDA 5, HZ1VFA 5
[t] supported by the Particle Physics and Astronomy Research Council, UK
[u] supported by the Korean Ministry of Education and Korea Science and Engineering Foundation
[v] supported by the Malaysian Ministry of Science, Technology and Innovation/Akademi Sains Malaysia grant SAGA 66-02-03-0048
[w] supported by the US National Science Foundation
[x] supported by the Polish State Committee for Scientific Research, grant no. 620/E-77/SPB/DESY/P-03/DZ 117/2003-2005 and grant no. 1P03B07427/2004-2006
[y] supported by the Polish Ministry of Scientific Research and Information Technology, grant no. 112/E-356/SPUB/DESY/P-03/DZ 116/2003-2005 and 1 P03B 065 27
[z] supported by the Japanese Ministry of Education, Culture, Sports, Science and Technology (MEXT) and its grants for Scientific Research
[aa] supported by FNRS and its associated funds (IISN and FRIA) and by an Inter-University Attraction Poles Programme subsidised by the Belgian Federal Science Policy Office
[ab] supported by the Spanish Ministry of Education and Science through funds provided by CICYT
[ac] supported by the Natural Sciences and Engineering Research Council of Canada (NSERC)
[ad] partially supported by the German Federal Ministry for Education and Research (BMBF)
[ae] supported by RF Presidential grant N 1685.2003.2 for the leading scientific schools and by the Russian Ministry of Education and Science through its grant for Scientific Research on High Energy Physics
[af] supported by the Netherlands Foundation for Research on Matter (FOM)
[ag] supported by the German-Israeli Foundation and the Israel Science Foundation
[ah] supported in part by the MINERVA Gesellschaft für Forschung GmbH, the Israel Science Foundation (grant no. 293/02-11.2) and the U.S.-Israel Binational Science Foundation

to zero (photoproduction), the additional contribution to prompt-photon events from the $gq \to q\gamma$ process, in which one of the initial partons comes from the photon which displays a hadronic structure (resolved process, Figs. 1c and d), can be dominant [1–5]. Prompt-photon measurements can be used to constrain the parton distribution functions (PDFs) of the proton and of the photon, as well as provide a testing ground for QCD calculations. A number of predictions exist [1–6] that can be confronted with the data.

The first observation by ZEUS of isolated photons accompanied by a hadronic jet in photoproduction used an integrated luminosity of $6.4\,\mathrm{pb}^{-1}$ [7]. Distributions sensitive to the intrinsic $k_{\mathrm{T}}$ in the $\gamma$+jet final state were later measured by ZEUS [8]. Inclusive prompt-photon cross sections with no jet requirement have also been reported [9]. Recently, H1 have published results on the $\gamma$+jet final state in photoproduction [10].

This paper reports the first ZEUS results on differential cross sections of the $\gamma$+jet final state in the photoproduction regime of $ep$ scattering. The cross sections are presented as a function of the transverse energy and pseudorapidity of both the photon ($E_{\mathrm{T}}^{\gamma}$, $\eta^{\gamma}$) and the jet ($E_{\mathrm{T}}^{\mathrm{jet}}$, $\eta^{\mathrm{jet}}$), as well as the fraction of the incoming photon momentum taken by the photon-jet system ($x_{\gamma}^{\mathrm{obs}}$). In contrast to previous measurements [7–10], the present analysis is based on the conversion-probability method, which uses information on the frequency with which photons convert to $e^+e^-$ in front of a dedicated preshower detector. Cross sections for $\gamma$+jet events are compared to next-to-leading-order (NLO) QCD, calculations based on the $k_{\mathrm{T}}$-factorisation approach and Monte Carlo (MC) models incorporating leading-order matrix elements plus parton showers. Since jets at relatively low $E_{\mathrm{T}}^{\mathrm{jet}}$ are measured in addition to the photon, parton-level calculations were corrected for hadronisation effects using a MC model. The hadronisation correction for $\gamma$+jet events is expected to be smaller than for dijets with similar jet transverse energies since the photon does not undergo hadronisation. Therefore, for low $E_{\mathrm{T}}^{\mathrm{jet}}$, the theoretical predictions for the $\gamma$+jet cross sections are expected to be more reliable than for dijet final states.

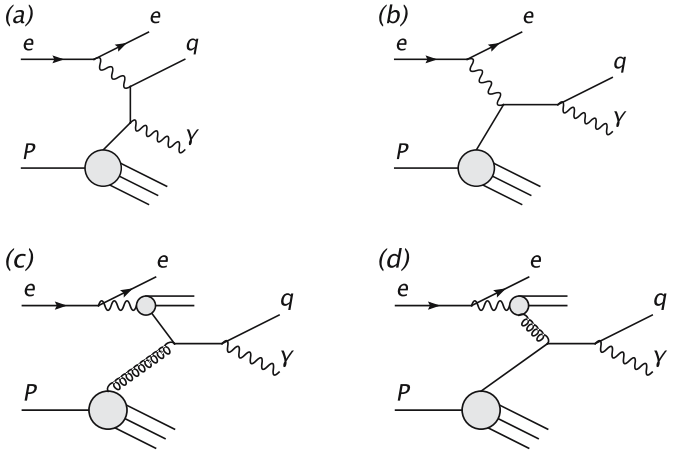


**Fig. 1.** Examples of diagrams for $\gamma+$jet events at leading order: direct photon interactions, (**a**, **b**) and resolved photon interactions, (**c**, **d**). The resolved diagrams with $t$-channel exchange are not shown

## 2 Data sample and experimental setup

The data sample was taken during the 1999-2000 period, corresponding to an integrated luminosity of $77.1 \pm 1.6\,\mathrm{pb}^{-1}$. The positron or electron beam energy was 27.5 GeV and the proton beam energy was 920 GeV, corresponding to a centre-of-mass energy of 318 GeV. Here and in the following, the term "electron" denotes generically both the electron ($e^-$) and the positron ($e^+$), unless otherwise stated.

ZEUS is a multipurpose detector described in detail elsewhere [11]. Of particular importance in the present study are the central tracking detector, the uranium-scintillator calorimeter and the barrel preshower detector.

The central tracking detector (CTD) [12–14] is a cylindrical drift chamber with nine super-layers covering the polar-angle[1] region $15^\circ < \theta < 164^\circ$ and the radial range 18.2–79.4 cm. Each super-layer consists of eight sense-wire layers. The transverse-momentum resolution for charged tracks traversing all CTD layers is $\sigma(p_{\mathrm{T}})/p_{\mathrm{T}} = 0.0058 p_{\mathrm{T}} \oplus 0.0065 \oplus 0.0014/p_{\mathrm{T}}$, with $p_{\mathrm{T}}$ in GeV.

The CTD is surrounded by the uranium-scintillator calorimeter, CAL [15–18], which is divided into three parts: forward, barrel and rear with the barrel consisting of 32 modules. The calorimeter is longitudinally segmented into electromagnetic (EMC) and hadronic (HAC) sections. The smallest subdivision of the CAL is called a cell. The energy resolution of the calorimeter under test-beam conditions is $\sigma_{\mathrm{E}}/E = 0.18/\sqrt{\mathrm{E}}$ for electrons and $\sigma_{\mathrm{E}}/E = 0.35/\sqrt{E}$ for hadrons, with $E$ in GeV.

The luminosity was measured using the bremsstrahlung process $ep \to ep\gamma$ with the luminosity monitor [19–21], a lead–scintillator calorimeter placed in the HERA tunnel at $Z = -107$ m.

The ZEUS barrel preshower detector (BPRE) [22] is located in front of the barrel calorimeter. The BPRE detector consists of 32 cassettes each containing 13 scintillator tiles of size $20 \times 20$ cm that were installed directly in front of each of the 32 barrel CAL modules. The measured output, calibrated in minimum ionising particle units (mips), is proportional to the energy loss of the incident particle after interaction with material (mainly the superconducting coil) in front of the barrel calorimeter.

The mip calibration of each of the 416 channels of the BPRE was done using all events triggered in the ZEUS detector. A luminosity of approximately $1\,\mathrm{pb}^{-1}$ was required for each calibration run. The one-mip signal was validated using cosmic-ray muon data. The single-mip resolution was

[1] The ZEUS coordinate system is a right-handed Cartesian system, with the $Z$ axis pointing in the proton beam direction, referred to as the "forward direction", and the $X$ axis pointing left towards the centre of HERA. The coordinate origin is at the nominal interaction point.

measured to be 0.3 mips and a minimum charge threshold corresponding to this value was applied to each channel. After calibration and correction for dead or inefficient channels, the signal efficiency for scattered electrons from deep-inelastic events was larger than 99%.

## 3 Theoretical predictions

The measured $\gamma$+jet cross sections were compared to NLO QCD based on collinear factorisation and DGLAP evolution [23–26], as well as to calculations based on the $k_{\mathrm{T}}$-factorisation approach with unintegrated quark and gluon densities.

A NLO calculation with additional higher-order terms was performed by Krawczyk and Zembrzuski (KZ) [4, 5]. The calculation includes the leading-order term $\gamma q \to \gamma q$, $\alpha_S$ corrections to this term, initial and final resolved-photon contributions, double-resolved contributions and the direct box diagram $\gamma g \to \gamma g$. The latter two contributions are calculated to order $\alpha_s^2$. No intrinsic transverse momentum of the initial-state partons in the proton was assumed. The renormalisation and factorisation scales for such calculation are set to $\mu_R = \mu_F = E_{\mathrm{T}}^{\gamma}$. The GRV parameterisation of the proton PDF [27], the photon PDF [28, 29] and the fragmentation function [30], were used.

A similar NLO calculation by Fontannaz, Guillet and Heinrich (FGH) [2, 3] contains additional higher-order corrections to the resolved photon process. For the FGH calculation, the MRST01 [31, 32] proton PDF and the AFG02 [33] photon PDF were used.

The prediction of A. Lipatov and N. Zotov (LZ) [6] is based on the $k_{\mathrm{T}}$-factorisation [34–36] method. The LZ calculation uses the unintegrated quark and gluon densities of the proton and photon according to the Kimber–Martin–Ryskin (KMR) prescription [37, 38] with the GRV parametrisations [27–29] of collinear quark and gluon densities. In this approach, both direct and resolved contributions are taken into account.

For all the calculations discussed, jets were reconstructed by running the longitudinally invariant $k_{\mathrm{T}}$ cluster algorithm in the inclusive mode [39, 40] on partons. A prompt-photon jet was defined as a jet containing the final-state photon. An isolation requirement, $E_{\mathrm{T}}^{\gamma,(\mathrm{true})} > 0.9 E_{\mathrm{T}}^{\gamma}$, where $E_{\mathrm{T}}^{\gamma,(\mathrm{true})}$ is the transverse energy of the final-state photon and $E_{\mathrm{T}}^{\gamma}$ is the total transverse energy of the prompt-photon jet, was applied to avoid the effects of collinear photon emission from quarks and to match the analysis isolation requirement (see Sect. 5). A comparison with NLO calculations based on a cone isolation requirement showed consistent results [41].

The calculations were corrected for hadronisation effects using the Pythia MC model discussed in Sect. 4. These corrections, which are negligible in the case of inclusive prompt photons, cannot be neglected when an accompanying jet is required. The hadronisation correction factors were defined as $C^{\mathrm{had}} = \sigma(\mathrm{hadrons})/\sigma(\mathrm{partons})$, where $\sigma$ denotes the differential cross sections calculated at the hadron and parton levels of the MC model, respectively. For both the parton and hadron levels of the MC generated events, the prompt photon was defined as the $k_{\mathrm{T}}$ jet with at least one photon and with the isolation requirement $E_{\mathrm{T}}^{\gamma,(\mathrm{true})} > 0.9\, E_{\mathrm{T}}^{\gamma}$. The $E_{\mathrm{T}}$ and $\eta$ distributions at the parton level in the MC model have a different shape than in the NLO calculations, especially at low $E_{\mathrm{T}}^{\gamma}$, where the NLO predictions rise faster than do those of the MC. To determine the hadronisation corrections, the MC parton distributions were reweighted to match the shapes of the NLO calculations. The reweighting was performed in four dimensions defined by the $E_{\mathrm{T}}^{\gamma}$, $\eta^{\gamma}$, $E_{\mathrm{T}}^{\mathrm{jet}}$ and $\eta^{\mathrm{jet}}$ variables.

The final hadronisation correction was determined from Pythia after the parton-level reweighting procedure discussed above. The Herwig model discussed in Sect. 4 requires a large reweighting so it was not used for the hadronisation correction.

The hadronisation correction factor for the total cross section in the kinematic range defined in Sect. 7 was 0.92. The corrections for the $\gamma$ + jet differential cross sections are close to unity for large transverse momenta of the photon, but they decrease to 0.78 at low $E_{\mathrm{T}}^{\gamma}$. It was verified that if no jet was required, the hadronisation corrections were close to unity.

The Pythia default setting includes a multiple-interaction simulation. It was verified that exclusion of multiple interactions from the parton-level of Pythia results in a negligible change in the hadronisation corrections.

## 4 Monte Carlo simulation

The measured cross sections were compared to leading-order Monte Carlo (MC) models which use the QCD parton shower approach to incorporate high-order QCD effects followed by fragmentation into hadrons. The MC events were generated with the Pythia 6.3 [42–44] and with the Herwig 6.5 [45, 46] models using the default parameters in each case. The CTEQ5L [47] proton PDF was used together with the SaS-2D parameterisation [48] for the photon PDF. Both direct and resolved prompt-photon events were generated.

The same MC samples were used to calculate the acceptance and to evaluate the signal and background content of the sample. Samples of background photoproduction events (without prompt-photon subprocesses) were generated in addition to the prompt photon samples. Both direct and resolved processes were simulated. These MC samples provided background photons from the decay of hadrons (predominantly from $\pi^0$ mesons).

The generated events were passed through a full simulation of the detector using Geant 3.13 [49] and processed with the same reconstruction program as used for the data. The MC samples after the detector simulation do not give a good description of the $E_{\mathrm{T}}$ and $\eta$ distributions seen in the data. Such discrepancies are most prominent at low $E_{\mathrm{T}}^{\gamma}$, and were attributed to an inadequacy of the MC models. For the acceptance calculations, the MC distributions were reweighted to match the distributions in $E_{\mathrm{T}}$ and $\eta$ of the

data. The reweighting was performed in four-dimensional phase space in $E_{\mathrm{T}}$ and $\eta$ of the photon and of the accompanying jet; thus correlations between these kinematic variables were properly taken into account.

## 5 Data selection and prompt-photon reconstruction

### 5.1 Event selection and jet reconstruction

The online selection made use of a standard ZEUS electron finding algorithm to select events with an electromagnetic cluster [7]. For the offline analysis, neutral-current deep inelastic (DIS) events with an identified scattered electron candidate were removed from the sample. This restricted the virtuality of the incident photon to the range $Q^2 < 1\,\mathrm{GeV}^2$. In addition, the following cuts were applied:

- charged current DIS events were rejected by requiring the total missing transverse momentum in the calorimeter to be less than 10 GeV;
- $0.2 < y_{\mathrm{JB}} < 0.8$, where $y_{\mathrm{JB}}$ is the inelasticity parameter reconstructed with the Jacquet–Blondel method [50];
- $|\, Z_{\mathrm{vertex}} \,| \leq 50\,\mathrm{cm}$, where $Z_{\mathrm{vertex}}$ is the event-vertex position determined from the tracks.

Jets were reconstructed by running the longitudinally invariant $k_{\mathrm{T}}$ algorithm in inclusive mode [39, 40] on energy-flow objects (EFOs) [51], which are based on a combination of track and calorimeter information. The jet variables $E_{\mathrm{T}}$ and $\eta$ were defined according to the Snowmass convention [52]. Each jet was classified as either a photon candidate or a hadronic jet. The photon-candidate jet was required to consist of EFOs without associated tracks and to be within the CTD and BCAL acceptance, $-0.74 < \eta^{\gamma} < 1.1$. For this jet, $E_{\mathrm{EMC}}/E_{\mathrm{tot}} > 0.9$ is required, where $E_{\mathrm{EMC}}$ is the energy reconstructed in the electromagnetic part of the CAL and $E_{\mathrm{tot}}$ is the total energy of this jet. After correction for energy losses, the cut $E_{\mathrm{T}}^{\gamma} > 5\,\mathrm{GeV}$ was applied.

Hadronic jets, after correction for energy losses, were selected in the kinematic range $E_{\mathrm{T}}^{\mathrm{jet}} > 6\,\mathrm{GeV}$, $-1.6 < \eta^{\mathrm{jet}} < 2.4$. They were required to have $E_{\mathrm{EMC}}/E_{\mathrm{tot}} < 0.9$. If more than one jet was found within the above kinematic cuts, the jet with the highest $E_{\mathrm{T}}^{\mathrm{jet}}$ was accepted. The minimum transverse momentum of the hadronic jet was set to be higher than for the photon candidate, since the NLO calculations employed in this analysis are unstable for symmetric cuts on the minimum transverse momenta of both jets [53, 54].

In total, 3910 events with a prompt-photon candidate and a hadronic jet were selected.

### 5.2 Identification of isolated photons and hadrons

For the prompt-photon identification, the conversion-probability method based on the BPRE was used. In contrast to the shower-profile approach used in previous measurements [7–9], the present approach uses the probability of conversion of photons to $e^+e^-$ pairs in detector elements and inactive material, mainly the solenoid located in front of the BCAL. The conversion probability for a single photon is lower than for multiphoton events arising from neutral meson decays ($\pi^0$, $\eta$, etc.); therefore, small BPRE signals can be used to identify isolated photons.

The response of the BPRE to single isolated photons was studied using the deeply virtual Compton scattering (DVCS) data, $ep \to e'\gamma p$, taken during 1999–2000. This sample is known to provide photons of high purity [55]. Events with two isolated electromagnetic clusters and one CTD track were pre-selected. One cluster was required to have energy $E_{e'} > 8\,\mathrm{GeV}$ and to be associated with the CTD track, thereby ensuring compatibility with the scattered electron. The cluster without an associated track was then reconstructed using the $k_{\mathrm{T}}$ cluster algorithm as described in Sect. 5.1. The photon candidate was required to be in the BCAL region, $-0.74 < \eta^{\gamma} < 1.1$, and to have energy in the range $5 < E_{\gamma} < 10\,\mathrm{GeV}$. The BPRE signal for the DVCS photons was determined as the sum of the signal of the BPRE tiles whose centre falls within a cone of size 0.7 in $\eta$-$\phi$ around the photon candidate. A smaller cone size leads to an efficiency that is not well reproduced by the MC. Other details of the DVCS selection and MC simulations are given elsewhere [55, 56].

In the DVCS sample, the fraction of events with BPRE signal below one mip is very sensitive to the amount of material in front of the BPRE since such events are dominated by non-converted photons. The MC simulation overestimates this fraction by 19% compared to the data due to an inadequate simulation of the material in front of the BPRE. This discrepancy does not have a significant dependence on the cone size.

The amount of inactive material was further studied using scattered electrons from DIS events. This study indicated that more material in front of the BCAL was necessary for the MC simulation.

Using a dedicated Geant simulation [49], it was found that an increase of inactive material in the MC simulation by $0.25\,X_0$ was sufficient to describe the fraction of events without photon conversions seen in the DVCS data. For this Geant simulation, it was assumed that all inactive material is distributed uniformly in the region of the ZEUS solenoid located in front of the BPRE tiles. The effect of the additional material was then taken into account in the standard ZEUS MC by applying a correction to the BPRE distribution based on the results of the dedicated simulation.

Figure 2 shows the BPRE signal for the DVCS data compared to the DVCS Monte Carlo model [56] after correction for additional material. There is good agreement between the data and the MC distribution. This shows that the inactive material and the BPRE resolution are well represented in the MC simulation.

The MC response of the BPRE to single hadrons was studied for $\pi^0$ and $\eta$ mesons. Since these mesons decay to several photons, more conversions to $e^+e^-$ will occur than for single photons. As expected, the average BPRE signal for $\pi^0$ and $\eta$ mesons was larger than for the isolated photons. An example of the MC simulation of the BPRE response to single $\gamma$, $\pi^0$ and $\eta$ is shown in Fig. 3. The BPRE

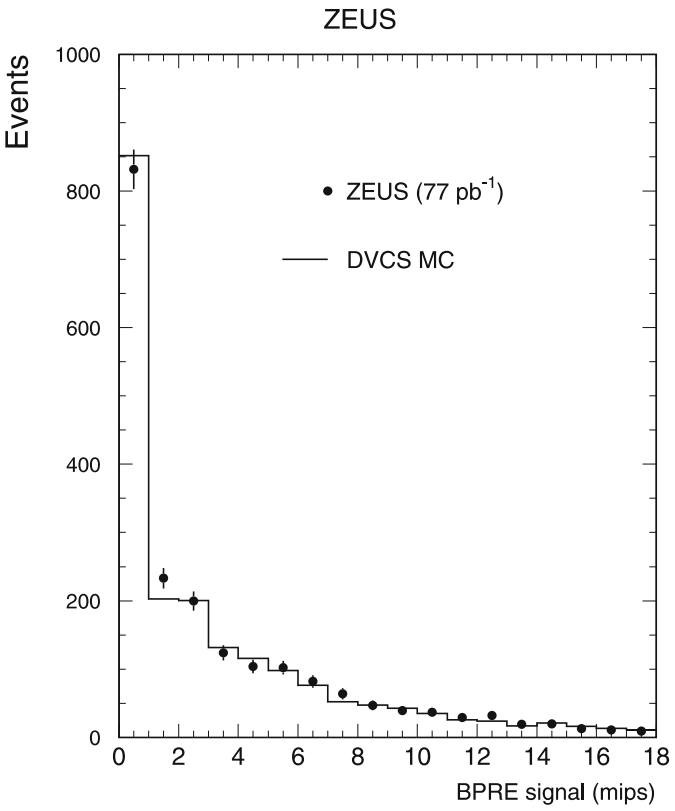


**Fig. 2.** The response of the BPRE detector to isolated photons in the DVCS data sample. The DVCS Monte Carlo distribution was normalised to the data

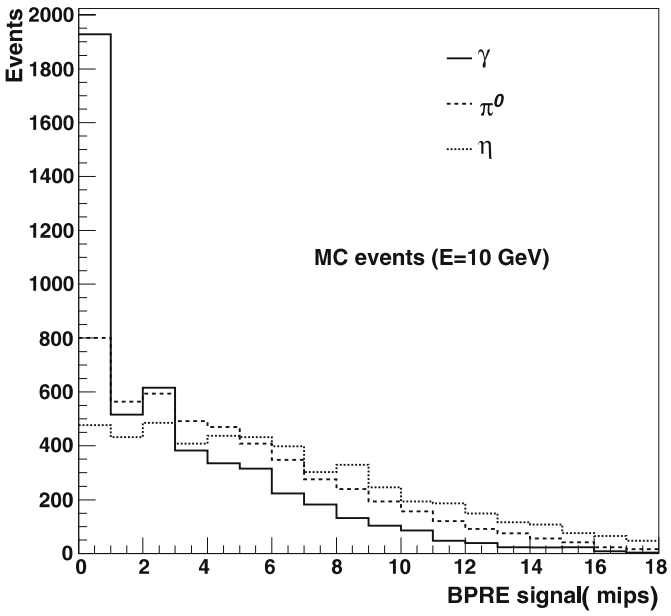


**Fig. 3.** The BPRE response to isolated photons, $\pi^0$ and $\eta$ in the MC simulation. An initial energy of 10 GeV for all particles was used. The amount of inactive material in front of the BPRE was set to $1.25X_0$

distributions for $\pi^0$ and $\eta$ mesons were also corrected to take into account additional dead material in front of the BPRE.

### 5.3 Extraction of the prompt-photon signal

The BPRE signal for prompt-photon candidates selected as described in Sect. 5.1 was determined using a cone of radius 0.7 in $\eta$-$\phi$ space, as was done for the DVCS analysis. Figure 4 shows the comparison between the data and the Pythia MC for: the BPRE signal for the photon candidate; the difference between the total calorimeter energy and the energies of the jet and the photon candidate, $\Delta E = E_{\rm tot} - E^{\rm jet} - E^{\gamma}$; and the distance from the photon candidate to any EFO in an event,

$$D = \sqrt{(\eta_\gamma - \eta_{\rm EFO})^2 + (\phi_\gamma - \phi_{\rm EFO})^2},$$

where $\eta_\gamma$ ($\eta_{\rm EFO}$) and $\phi_\gamma$ ($\phi_{\rm EFO}$) are the azimuthal angle and pseudorapidity of the photon candidate (EFO).

Figure 4a shows that there is a significant fraction of events with a small number of mips, similar to the DVCS data. However, since the dijet photoproduction cross section is higher by several orders of magnitude than the $\gamma$+jet cross section, there is additional hadronic background even after the cuts discussed in Sect. 5.1.

The BPRE distribution for the prompt-photon candidates was used to determine the background fraction. The

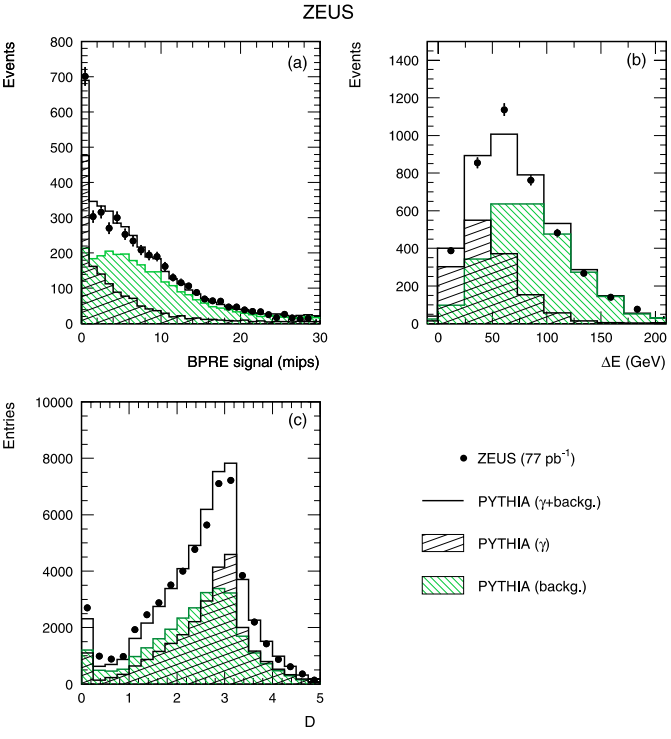


**Fig. 4.** Comparisons between the data and MC for: **a** the BPRE signal for the photon candidate; **b** the difference between the total calorimeter energy and the energies of the jet and the photon candidate, $\Delta E = E_{\rm tot} - E^{\rm jet} - E^{\gamma}$; and **c** the distance from the photon candidate to any EFO (see the text). The non-hatched histogram is the sum of the prompt photon MC and the background MC. The fraction of the prompt-photon events was found after a $\chi^2$ minimisation procedure for the BPRE distribution shown in **a**

fraction of inclusive dijet photoproduction events needed was found from a $\chi^2$-minimisation procedure. After the inclusion of the background events, the shape of the BPRE distribution for the prompt-photon candidates is well reproduced by the MC simulation, as shown in Fig. 4a.

The inclusion of the dijet background leads to good description of the CAL distributions shown in Fig. 4b and c, which are also sensitive to the prompt-photon events. On average, the $\Delta E$ should be larger for the dijet events, where more energy is radiated outside the dijet system than for the $\gamma$+jet events. After the inclusion of the background, this distribution is well reproduced by MC.

The background fraction described above was used in the calculation of the total $\gamma$+jet cross section. For differential cross sections, the background fractions were determined by fitting the BPRE signal independently in each bin of the respective distributions. In order to reduce statistical fluctuations in regions of small statistics, it was assumed that the background fractions varied smoothly from bin to bin. Therefore, the dependence of the background fraction on $E_{\mathrm{T}}^{\gamma}$, $\eta^{\gamma}$, $E_{\mathrm{T}}^{\mathrm{jet}}$, $\eta^{\mathrm{jet}}$ and $x_{\gamma}^{\mathrm{obs}}$ was obtained by fitting the background fractions for each bin with a linear function. The number of prompt-photon events in each kinematic bin was determined from such a linear-regression fit. The statistical uncertainties on the number of signal events were evaluated using 68% confidence-level limits on the linear fit of the fractions.

## 6 Cross section calculations and systematic uncertainties

The differential cross sections for a given observable $Y$ were determined as:

$$\frac{\mathrm{d}\sigma}{\mathrm{d}Y} = \frac{N}{A \cdot \mathcal{L} \cdot \Delta Y} \ ,$$

where $N$ is the number of prompt-photon events in a bin of size $\Delta Y$, $A$ is the acceptance and $\mathcal{L}$ is the integrated luminosity. The acceptance was calculated using MC from the ratio of the number of reconstructed events after the selection cuts to the number of generated events.

The systematic uncertainties were evaluated by changing the selection and the analysis procedure. The contribution of each cut variation to the total cross section is given in parentheses as a percentage of the total cross section:

- the calorimeter energy scale was changed by $\pm 3\%$ ($^{+9.1}_{-11.7}\%$);
- the transverse momentum cut and the $\eta$ range for the photon and hadron jet were lowered (raised) independently by one $\sigma$ of the resolution. The systematic uncertainty due to the transverse-energy cut for the photon was found to be ($^{+2.5}_{-3.7}\%$). The largest systematical uncertainty due to the transverse-energy cut on the jet was ($^{+2.2}_{-2.0}\%$). The systematic uncertainty associated with the variations in the pseudorapidity was small ($\pm 0.8\%$);
- the uncertainty in the quantity of inactive material in the MC was estimated by varying the amount of inactive material by $\pm 5\%$ of a $\mathrm{X}_0$ in the Geant-based correction factors ($^{-7.0}_{+5.0}\%$);
- the cone radius for the determination of the BPRE signal was changed by $\pm 0.1$ units ($^{-2.3}_{+2.7}\%$). A larger cone size leads to a larger leakage of hadronic energy into the photon, which is not well simulated in MC;
- variations of the cuts on $y_{\mathrm{JB}}$, $Z_{\mathrm{vertex}}$ and on total missing transverse energy ($\pm 2\%$);
- the resolved contribution in MC was changed by $\pm 15\%$ ($< 1\%$);
- the cut on the electromagnetic fraction $E_{\mathrm{EMC}}/E_{\mathrm{tot}}$ for the photon jet was changed by $\pm 0.02$ ($^{+0.9}_{-1.5}\%$);
- the acceptance correction and the fraction of background photoproduction events was determined using Herwig ($-0.6\%$).

The overall systematic uncertainty was determined by adding the above uncertainties in quadrature. A 2% normalisation uncertainty due to the luminosity measurement error was not included in the systematic uncertainties.

As an additional check, the differential $\gamma$+jet cross sections were found by using the global background fraction determined in the full kinematic range. Further, the cross sections were calculated from the number of the detector-level events in the data and MC after requiring a BPRE signal $< 7$ mip, i.e. in a region where the purity of the prompt photon sample is expected to be above 50%. The results from these alternative methods were consistent with the final cross sections.

## 7 Results

The total cross section for the process $ep \to e + \gamma_{\mathrm{prompt}} + \mathrm{jet} + X$ for $0.2 < y < 0.8$, $Q^2 < 1\,\mathrm{GeV}^2$, $5 < E_{\mathrm{T}}^{\gamma} < 16\,\mathrm{GeV}$, $6 < E_{\mathrm{T}}^{\mathrm{jet}} < 17\,\mathrm{GeV}$, $-0.74 < \eta^{\gamma} < 1.1$, $-1.6 < \eta^{\mathrm{jet}} < 2.4$ and $E_{\mathrm{T}}^{\gamma,(\mathrm{true})} > 0.9\,E_{\mathrm{T}}^{\gamma}$ was measured to be

$$\begin{aligned}\sigma(ep \to e + \gamma_{\mathrm{prompt}} + \mathrm{jet} + X) \\ = 33.1 \pm 3.0\,(\mathrm{stat.})\,^{+4.6}_{-4.2}(\mathrm{syst.})\,\mathrm{pb}\,.\end{aligned}$$

This cross section should be compared to the QCD predictions after the hadronisation corrections: $23.3^{+1.9}_{-1.7}\,\mathrm{pb}$ (KZ), $23.5^{+1.7}_{-1.6}\,\mathrm{pb}$ (FGH) and $30.7^{+3.2}_{-2.7}\,\mathrm{pb}$ (LZ). The scale uncertainties on the QCD calculations were estimated by varying $\mu_R$ between $\mu_R/2$ and $2\mu_R$. The Pythia and Herwig cross sections are 20.0 pb and 13.5 pb, respectively.

The differential cross sections as functions of $E_{\mathrm{T}}$ and $\eta$ for the prompt-photon candidates and for the accompanying jets are shown in Figs. 5 and 6. Figure 7 shows the distribution for $x_{\gamma}^{\mathrm{obs}}$ defined as $\sum_{\gamma,\mathrm{jet}}(E_i - P_Z^i)/(2E_e y)$ (the sum runs over the photon candidate and the hadronic jet). Table 1 gives the differential cross sections with the statistical and systematical uncertainties, as well as the hadronisation-correction factors calculated in the same bins as the data[2].

[2] The actual hadronisation corrections applied to the NLO calculations shown in Figs. 5–9 were calculated using finer bins.

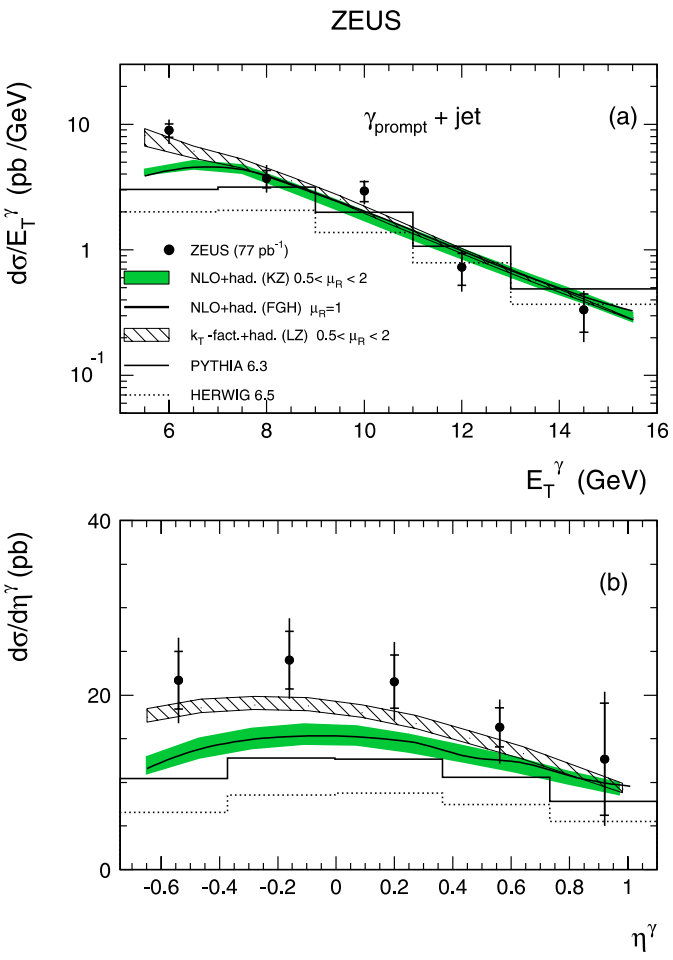


**Fig. 5.** The $\gamma+$jet differential cross sections as functions of $E_{\mathrm{T}}^{\gamma}$ and $\eta^{\gamma}$ compared to theoretical QCD calculations (with hadronisation corrections included). The *histograms* show the predictions of the Monte Carlo models. The *inner error bars* show the statistical uncertainties, the *outer ones* show statistical and systematic uncertainties added in quadrature. The shaded bands for the KZ prediction correspond to the uncertainty in the renormalisation scale which was changed by a factor of 0.5 and 2. A similar uncertainty exists for the FGH prediction (not shown)

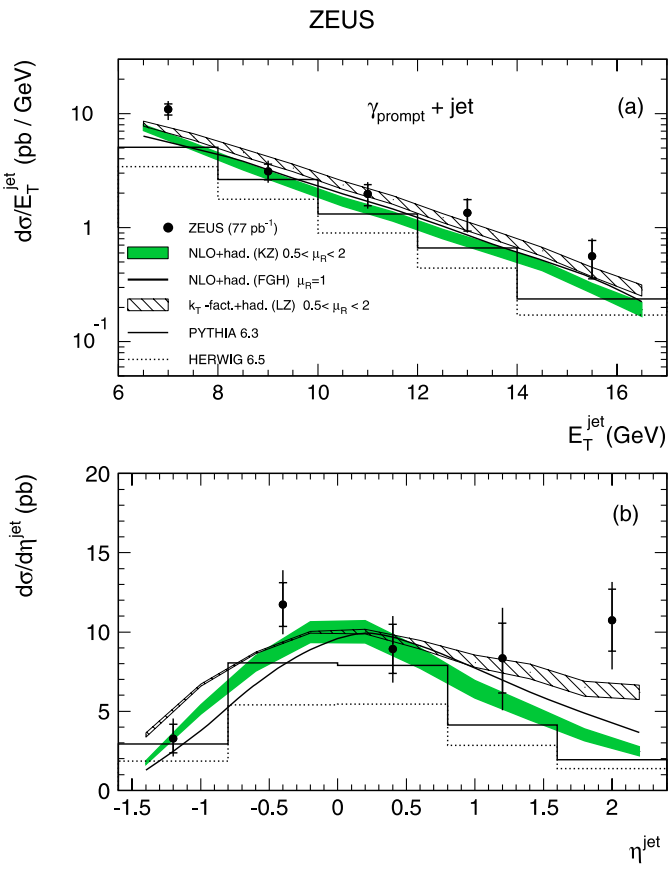


**Fig. 6.** The $\gamma+$jet differential cross sections as functions of $E_T^{\mathrm{jet}}$ and $\eta^{\mathrm{jet}}$ compared to the QCD calculations (with hadronisation corrections) and Monte Carlo models

The Pythia and Herwig differential cross sections do not rise as steeply at low $E_{\mathrm{T}}^{\gamma}$ as do the data. In addition, they underestimate the measured cross sections. The KZ NLO prediction, corrected for hadronisation effects as described in Sect. 3, describes the data better. However, it underestimates the observed cross section at low $E_{\mathrm{T}}^{\gamma}$ and in the forward jet region. The observed difference between the data and the NLO QCD calculations is concentrated in the $x_{\gamma}^{\mathrm{obs}} < 0.75$ region which is sensitive to the resolved photon contribution.

The FGH prediction is similar to the KZ NLO. The largest difference between the two predictions is found for the $\eta^{\mathrm{jet}}$ cross section, where the FGH cross section is closer to the data in the forward jet region. The renormalisation scale uncertainty for the FGH QCD calculations is similar to that estimated for the KZ predictions (not shown).

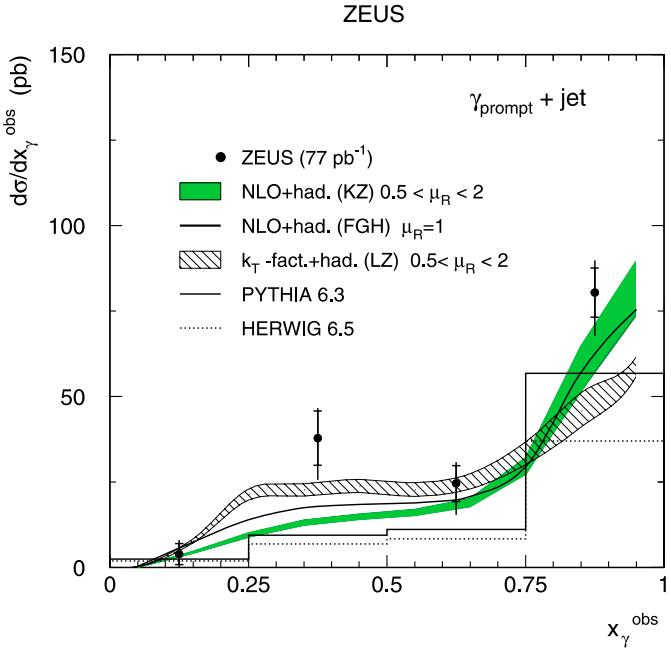


**Fig. 7.** The $x_{\gamma}^{\mathrm{obs}}$ cross section for $\gamma+$jet events compared to the NLO QCD calculations (with hadronisation corrections) and Monte Carlo models

**Table 1.** The differential prompt-photon cross sections with additional jet requirement measured in the region $0.2 < y < 0.8$, $Q^2 < 1\,\mathrm{GeV}^2$, $5 < E_\mathrm{T}^\gamma < 16\,\mathrm{GeV}$, $6 < E_\mathrm{T}^{jet} < 17\,\mathrm{GeV}$, $-0.74 < \eta^\gamma < 1.1$ and $-1.6 < \eta^{jet} < 2.4$. The statistical and systematical uncertainties are given separately. The hadronisation correction factors (see the text) applied to the QCD calculations for the same kinematic bins as for the data are also shown

| $E_\mathrm{T}^\gamma$ (GeV) | $\mathrm{d}\sigma/\mathrm{d}E_\mathrm{T}^\gamma$ (pb/GeV) | $C^\mathrm{had}$ |
|---|---|---|
| 5.00, 7.00 | $9.0 \pm 1.1^{+1.6}_{-1.7}$ | 0.78 |
| 7.00, 9.00 | $3.7 \pm 0.6^{+0.9}_{-0.6}$ | 1.01 |
| 9.00, 11.00 | $2.9 \pm 0.5^{+0.3}_{-0.4}$ | 1.05 |
| 11.00, 13.00 | $0.7 \pm 0.2^{+0.2}_{-0.2}$ | 1.06 |
| 13.00, 16.00 | $0.3 \pm 0.1^{+0.1}_{-0.1}$ | 1.06 |
| $\eta^\gamma$ | $\mathrm{d}\sigma/\mathrm{d}\eta^\gamma$ (pb) | $C^\mathrm{had}$ |
| −0.74, −0.34 | $21.7 \pm 3.3^{+3.6}_{-3.7}$ | 0.89 |
| −0.34, 0.02 | $24.0 \pm 3.3^{+3.5}_{-2.9}$ | 0.91 |
| 0.02, 0.38 | $21.5 \pm 3.0^{+3.4}_{-3.2}$ | 0.93 |
| 0.38, 0.74 | $16.3 \pm 2.3^{+2.2}_{-3.5}$ | 0.95 |
| 0.74, 1.10 | $12.7 \pm 6.4^{+4.3}_{-4.2}$ | 0.95 |
| $E_\mathrm{T}^\mathrm{jet}$ (GeV) | $\mathrm{d}\sigma/\mathrm{d}E_\mathrm{T}^\mathrm{jet}$ (pb/GeV) | $C^\mathrm{had}$ |
| 6.00, 8.00 | $10.9 \pm 1.2^{+1.5}_{-1.8}$ | 0.89 |
| 8.00, 10.00 | $3.1 \pm 0.5^{+0.6}_{-0.4}$ | 0.96 |
| 10.00, 12.00 | $2.0 \pm 0.4^{+0.3}_{-0.3}$ | 0.97 |
| 12.00, 14.00 | $1.3 \pm 0.4^{+0.2}_{-0.2}$ | 0.95 |
| 14.00, 17.00 | $0.6 \pm 0.2^{+0.1}_{-0.0}$ | 0.90 |
| $\eta^\mathrm{jet}$ | $\mathrm{d}\sigma/\mathrm{d}\eta^\mathrm{jet}$ (pb) | $C^\mathrm{had}$ |
| −1.60, −0.80 | $3.3 \pm 0.9^{+0.9}_{-0.7}$ | 0.74 |
| −0.80, 0.00 | $11.7 \pm 1.4^{+1.7}_{-1.3}$ | 0.85 |
| 0.00, 0.80 | $8.9 \pm 1.5^{+1.4}_{-1.5}$ | 0.99 |
| 0.80, 1.60 | $8.3 \pm 2.2^{+2.3}_{-2.4}$ | 1.07 |
| 1.60, 2.40 | $10.7 \pm 2.0^{+1.4}_{-2.4}$ | 1.09 |
| $x_\gamma^\mathrm{obs}$ | $\mathrm{d}\sigma/\mathrm{d}x_\gamma^\mathrm{obs}$ (pb) | $C^\mathrm{had}$ |
| 0.00, 0.25 | $3.9 \pm 3.1^{+4.2}_{-4.2}$ | 0.91 |
| 0.25, 0.50 | $37.9 \pm 7.9^{+8.8}_{-12.3}$ | 0.95 |
| 0.50, 0.75 | $24.5 \pm 5.2^{+6.3}_{-9.2}$ | 1.06 |
| 0.75, 1.00 | $80.4 \pm 7.2^{+9.4}_{-12.6}$ | 0.90 |

The LZ prediction based on the $k_\mathrm{T}$-factorisation approach corrected for hadronisation effects gives the best description of the $E_\mathrm{T}$ and $\eta$ cross sections. In particular, it describes the lowest $E_\mathrm{T}^\gamma$ region better than the KZ and FGH NLO predictions. The $\eta^\mathrm{jet}$ cross section for the associated jet in the forward region is also better reproduced by the LZ calculation.

**Table 2.** The differential prompt-photon cross sections with additional jet requirement measured in the region defined as for Table 1 except for the cut on the transverse energy of the prompt photon, which was increased to 7 GeV. The statistical and systematical uncertainties are given separately. The hadronisation correction factors applied to the QCD calculations for the same kinematic bins as for the data are also shown

| $\eta^\gamma$ | $\mathrm{d}\sigma/\mathrm{d}\eta^\gamma$ (pb) | $C^\mathrm{had}$ |
|---|---|---|
| −0.74, −0.34 | $5.0 \pm 0.9^{+1.1}_{-0.7}$ | 0.99 |
| −0.34, 0.02 | $8.2 \pm 1.3^{+1.6}_{-1.4}$ | 1.00 |
| 0.02, 0.38 | $9.0 \pm 1.4^{+1.4}_{-1.2}$ | 1.02 |
| 0.38, 0.74 | $7.9 \pm 1.6^{+1.2}_{-1.3}$ | 1.04 |
| 0.74, 1.10 | $8.0 \pm 2.7^{+0.7}_{-2.7}$ | 1.05 |
| $E_\mathrm{T}^\mathrm{jet}$ (GeV) | $\mathrm{d}\sigma/\mathrm{d}E_\mathrm{T}^\mathrm{jet}$ (pb/GeV) | $C^\mathrm{had}$ |
| 6.00, 8.00 | $2.5 \pm 0.4^{+0.4}_{-0.4}$ | 1.08 |
| 8.00, 10.00 | $2.0 \pm 0.4^{+0.3}_{-0.2}$ | 1.00 |
| 10.00, 12.00 | $1.3 \pm 0.2^{+0.2}_{-0.2}$ | 0.99 |
| 12.00, 14.00 | $0.5 \pm 0.2^{+0.1}_{-0.1}$ | 0.97 |
| 14.00, 17.00 | $0.2 \pm 0.1^{+0.1}_{-0.0}$ | 0.91 |
| $\eta^\mathrm{jet}$ | $\mathrm{d}\sigma/\mathrm{d}\eta^\mathrm{jet}$ (pb) | $C^\mathrm{had}$ |
| −1.60, −0.80 | $1.1 \pm 0.3^{+0.3}_{-0.4}$ | 0.85 |
| −0.80, 0.00 | $4.2 \pm 0.7^{+0.4}_{-0.5}$ | 0.95 |
| 0.00, 0.80 | $5.6 \pm 1.0^{+0.8}_{-0.6}$ | 1.06 |
| 0.80, 1.60 | $3.4 \pm 0.8^{+0.8}_{-0.6}$ | 1.15 |
| 1.60, 2.40 | $1.8 \pm 0.5^{+0.6}_{-0.5}$ | 1.18 |
| $x_\gamma^\mathrm{obs}$ | $\mathrm{d}\sigma/\mathrm{d}x_\gamma^\mathrm{obs}$ (pb) | $C^\mathrm{had}$ |
| 0.00, 0.25 | $1.6 \pm 0.9^{+2.1}_{-1.7}$ | 1.15 |
| 0.25, 0.50 | $7.3 \pm 1.5^{+2.0}_{-3.1}$ | 1.11 |
| 0.50, 0.75 | $9.1 \pm 1.6^{+2.5}_{-1.7}$ | 1.16 |
| 0.75, 1.00 | $33.9 \pm 4.4^{+5.3}_{-5.5}$ | 0.99 |

It is difficult to compare the present cross sections with the H1 result [10], since a significant model-dependent extrapolation to the low $E_\mathrm{T}^\mathrm{jet}$ region used by H1 is required. A comparison in the region $E_\mathrm{T}^\mathrm{jet} > 6$ GeV shows good agreement with H1 for the $E_\mathrm{T}^\mathrm{jet}$ differential cross section.

Since the largest difference between the NLO calculations and the data is concentrated in the region of low $E_\mathrm{T}^\gamma$ and low $E_\mathrm{T}^\mathrm{jet}$, it is instructive to verify the level of agreement with NLO when the minimum transverse energy of the detected prompt photons is increased from 5 GeV to 7 GeV. In this case, hadronisation corrections are expected to be smaller. Further, in comparison with the previous measurements, such a choice may emphasize different aspect of contributions of high-order QCD radiation [54], since the transverse energy of the prompt-photon is larger than that of the jet.

The total $ep \to e + \gamma_\mathrm{prompt} + \mathrm{jet} + X$ cross section for $E_\mathrm{T}^\gamma > 7$ GeV (keeping the other cuts the same as before) is

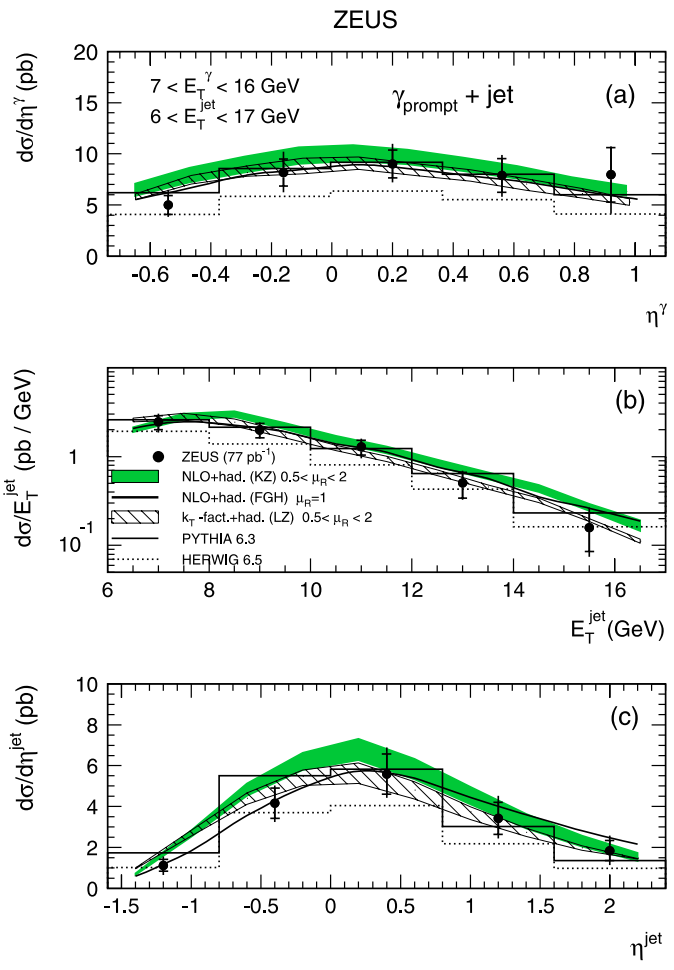


**Fig. 8.** The differential $\gamma+$jet cross sections as functions of: **a** $\eta^{\gamma}$, **b** $E_{\mathrm{T}}^{\mathrm{jet}}$ and **c** $\eta^{\mathrm{jet}}$ compared to the QCD calculations (with hadronisation corrections) and Monte Carlo models. The cuts are the same as for Figs. 5 and 6, except for the cut on the transverse energy of the prompt photons, which was increased to 7 GeV

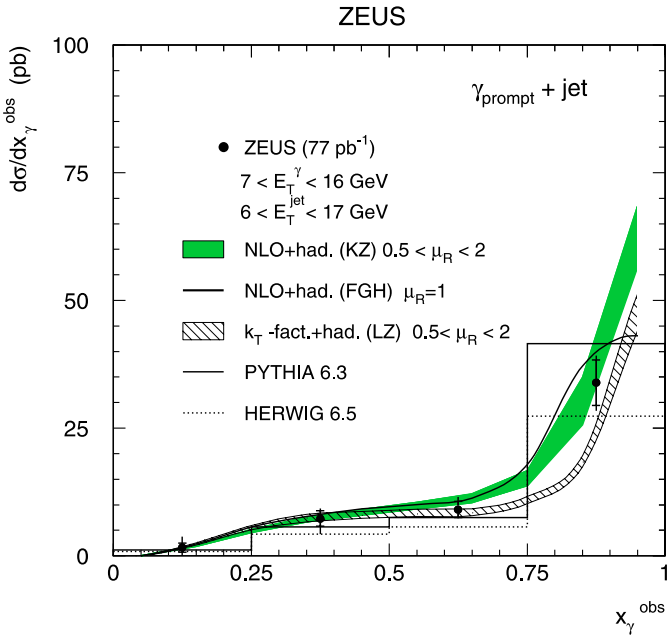


**Fig. 9.** The $x_{\gamma}^{\mathrm{obs}}$ cross section for $\gamma+$jet events compared to the QCD calculations (with hadronisation corrections) and Monte Carlo models. The cuts are the same as for Fig. 7 except for the cut on the transverse energy of the prompt photon which was increased to 7 GeV

$\sigma = 13.8 \pm 1.2\,(\mathrm{stat.})\,^{+1.8}_{-1.6}(\mathrm{syst.})\,\mathrm{pb}$. This result agrees with the QCD calculations after the hadronisation corrections: $14.9^{+1.3}_{-1.0}\,\mathrm{pb}$ (KZ), $13.4^{+1.1}_{-0.9}\,\mathrm{pb}$ (FGH) and $13.6^{+0.9}_{-1.0}\,\mathrm{pb}$ (LZ). The PYTHIA and HERWIG models predict 13.7 pb and 9.4 pb, respectively.

Figures 8 and 9 and Table 2 show the corresponding differential cross sections. The applied hadronisation corrections are given in Table 2. For the $E_{\mathrm{T}}^{\gamma} > 7$ GeV cut, both the NLO QCD and the LZ predictions agree well with the data. The Pythia MC model also agrees well with the cross sections, while Herwig is still below the data.

## 8 Conclusions

The photoproduction of prompt photons, together with an accompanying jet, has been measured in $ep$ collisions at a centre-of-mass energy of 318 GeV with the ZEUS detector at HERA using an integrated luminosity of $77\,\mathrm{pb}^{-1}$.

In the kinematic region $E_{\mathrm{T}}^{\gamma} > 5$ GeV and $E_{\mathrm{T}}^{\mathrm{jet}} > 6$ GeV the prompt-photon data disagree with the available MC predictions which predict a less steep rise of the cross sections with decreasing $E_{\mathrm{T}}^{\gamma}$. The discrepancy is reduced for the NLO calculations. However, they still underestimate the data in the low $E_{\mathrm{T}}^{\gamma}$ and $E_{\mathrm{T}}^{\mathrm{jet}}$ regions, which are likely to be the most sensitive to the treatment of high-order QCD terms and hadronisation effects. The best description of the data was found for the calculations based on the $k_{\mathrm{T}}$-factorisation approach and unintegrated parton densities.

When the minimum transverse energy of prompt photons is increased from 5 GeV to 7 GeV, both NLO QCD and the $k_{\mathrm{T}}$-factorisation calculations describe the data well.

*Acknowledgements.* We thank the DESY Directorate for their strong support and encouragement. The remarkable achievements of the HERA machine group were essential for the successful completion of this work and are greatly appreciated. We are grateful for the support of the DESY computing and network services. The design, construction and installation of the ZEUS detector have been made possible owing to the ingenuity and effort of many people from DESY and home institutes who are not listed as authors. We thank M. Fontannaz, G. Heinrich, M. Krawczyk, A. Lipatov and A. Zembrzuski for discussions and for providing the QCD calculations.

## References

1. L.E. Gordon, W. Vogelsang, Phys. Rev. D **52**, 58 (1995)
2. M. Fontannaz, J.P. Guillet, G. Heinrich, Eur. Phys. J. C **21**, 303 (2001)

3. M. Fontannaz, G. Heinrich, Eur. Phys. J. C **34**, 191 (2004)
4. M. Krawczyk, A. Zembrzuski, Phys. Rev. D **64**, 14 017 (2001)
5. A. Zembrzuski, M. Krawczyk, preprint hep-ph/0309308, 2003
6. A.V. Lipatov, N.P. Zotov, Phys. Rev. D **72**, 054 002 (2005)
7. ZEUS Collaboration, J. Breitweg et al., Phys. Lett. B **413**, 201 (1997)
8. ZEUS Collaboration, S. Chekanov et al., Phys. Lett. B **511**, 19 (2001)
9. ZEUS Collaboration, J. Breitweg et al., Phys. Lett. B **472**, 175 (2000)
10. H1 Collaboration, A. Aktas et al., Eur. Phys. J. C **38**, 437 (2005)
11. ZEUS Collaboration, U. Holm (ed.), The ZEUS Detector, (Status Report (unpublished), DESY, 1993), available on http://www-zeus.desy.de/bluebook/bluebook.html
12. N. Harnew et al., Nucl. Instrum. Methods A **279**, 290 (1989)
13. B. Foster et al., Nucl. Phys. Proc. Suppl. B **32**, 181 (1993)
14. B. Foster et al., Nucl. Instrum. Methods A **338**, 254 (1994)
15. M. Derrick et al., Nucl. Instrum. Methods A **309**, 77 (1991)
16. A. Andresen et al., Nucl. Instrum. Methods A **309**, 101 (1991)
17. A. Caldwell et al., Nucl. Instrum. Methods A **321**, 356 (1992)
18. A. Bernstein et al., Nucl. Instrum. Methods A **336**, 23 (1993)
19. J. Andruszków et al., Preprint DESY-92-066, DESY (1992)
20. ZEUS Collaboration, M. Derrick et al., Z. Phys. C **63**, 391 (1994)
21. J. Andruszków et al., Acta Phys. Pol. B **32**, 2025 (2001)
22. S. Magill, S. Chekanov, Proceedings of the IX Int. Conference on Calorimetry (Annecy, Oct 9–14, 2000), B. Aubert et al. (Ed.), p. 625. Frascati Physics Series 21, Annecy, France (2001)
23. V.N. Gribov, L.N. Lipatov, Sov. J. Nucl. Phys. **15**, 438 (1972)
24. L.N. Lipatov, Sov. J. Nucl. Phys. **20**, 94 (1975)
25. Y.L. Dokshitzer, Sov. Phys. JETP **46**, 641 (1977)
26. G. Altarelli, G. Parisi, Nucl. Phys. B **126**, 298 (1977)
27. M. Glück, E. Reya, A. Vogt, Z. Phys. C **67**, 433 (1995)
28. M. Glück, E. Reya, A. Vogt, Phys. Rev. D **45**, 3986 (1992)
29. M. Glück, E. Reya, A. Vogt, Phys. Rev. D **46**, 1973 (1992)
30. M. Glück, E. Reya, A. Vogt, Phys. Rev. D **48**, 116 (1993)
31. A.D. Martin et al., Eur. Phys. J. C **14**, 133 (2000)
32. A.D. Martin et al., Eur. Phys. J. C **23**, 73 (2002)
33. P. Aurenche, J.P. Guillet, M. Fontannaz, Z. Phys. C **64**, 621 (1994)
34. E.M. Levin et al., Sov. J. Nucl. Phys. **53**, 657 (1991)
35. S. Catani, M. Ciafaloni, F. Hautmann, Nucl. Phys. B **366**, 135 (1991)
36. J.C. Collins, R.K. Ellis, Nucl. Phys. B **360**, 3 (1991)
37. M.A. Kimber, A.D. Martin, M.G. Ryskin, Phys. Rev. D **63**, 114 027 (2001)
38. G. Watt, A.D. Martin, M.G. Ryskin, Eur. Phys. J. C **31**, 73 (2003)
39. S.D. Ellis, D.E. Soper, Phys. Rev. D **48**, 3160 (1993)
40. S. Catani et al., Nucl. Phys. B **406**, 187 (1993)
41. A. Zembrzuski, Private communication
42. M. Bengtsson, T. Sjöstrand, Comput. Phys. Commun. **46**, 43 (1987)
43. T. Sjöstrand, Comput. Phys. Commun. **82**, 74 (1994)
44. T. Sjöstrand et al., Comput. Phys. Commun. **135**, 238 (2001)
45. G. Marchesini et al., Comput. Phys. Commun. **67**, 465 (1992)
46. G. Corcella et al., JHEP **1**, 10 (2001)
47. CTEQ Collaboration, H.L. Lai et al., Eur. Phys. J. C **12**, 375 (2000)
48. G.A. Schuler, T. Sjöstrand, Phys. Lett. B **376**, 193 (1996)
49. R. Brun et al., Geant3, Technical Report CERN-DD/EE/84-1, CERN, 1987
50. F. Jacquet, A. Blondel, Proceedings of the Study for an *ep* Facility for Europe, U. Amaldi (ed.), p. 391. (Hamburg, Germany, 1979). Also in preprint DESY 79/48
51. G.M. Briskin, Diffractive Dissociation in *ep* Deep Inelastic Scattering. (Ph.D. Thesis, Tel Aviv University, 1998)
52. J.E. Huth et al., Research Directions for the Decade. Proceedings of Summer Study on High Energy Physics, 1990, E.L. Berger (Ed.), p. 134. (World Scientific, 1992). Also in preprint FERMILAB-CONF-90-249-E
53. S. Frixione, G. Ridolfi, Nucl. Phys. B **507**, 315 (1997)
54. M. Fontannaz, J.P. Guillet, G. Heinrich, Eur. Phys. J. C **22**, 303 (2001)
55. ZEUS Collaboration, S. Chekanov et al., Phys. Lett. B **573**, 46 (2003)
56. P.R.B. Saull, A Monte Carlo Generator for Deeply Virtual Compton Scattering at HERA, 1999, available on http://www-zeus.desy.de/physics/diff/pub/MC